North Australian Sea Surface Temperatures and the El Niño–Southern Oscillation in Observations and Models

JENNIFER L. CATTO AND NEVILLE NICHOLLS

School of Geography and Environmental Science, Monash University, Clayton, Victoria, Australia

CHRISTIAN JAKOB

School of Mathematical Science, Monash University, Clayton, Victoria, Australia

(Manuscript received 23 May 2011, in final form 22 November 2011)

ABSTRACT

Interannual variations in the sea surface temperature (SST) to the north of Australia are strongly linked to variations in Australian climate, including winter rainfall and tropical cyclone numbers. The north Australian SSTs are also closely linked to ENSO and tropical Pacific SSTs, with the relationship exhibiting a strong seasonal cycle. Credible predictions of Australian climate change therefore depend on climate models being able to represent ENSO and its connection to north Australian SSTs, the topic of this study.

First, the observational datasets of the Met Office Hadley Centre Sea Ice and Sea Surface Temperature (HadISST) and the NOAA Extended Reconstructed Sea Surface Temperature (ERSST) are used to document the links between the Niño-3.4 index and a north Australian SST index, and the temporal evolution of north Australian SSTs during ENSO events. During austral autumn, the correlation between Niño-3.4 SST and north Australian SST is positive, while in austral spring it is strongly negative. During El Niño events, the north Australian SST anomalies become negative in the austral spring preceding the development of the positive Niño-3.4 SST anomalies.

The coupled models participating in the Coupled Model Intercomparison Project phase 3 (CMIP3) are evaluated in terms of this temporal evolution of Niño-3.4 SST and the relationship to north Australian SST for the twentieth-century simulations. Some of the models perform very well, while some do not capture the seasonal cycle of correlations at all. The way in which these relationships may change in the future is examined using the A2 emissions scenario in those models that do a reasonable job of capturing the present-day observed relationship, and very little change is found.

1. Introduction

Interannual variations in sea surface temperatures (SSTs) around northern Australia are closely related to interannual variations in the Australian climate (e.g., Nicholls 1984a,c; Ummenhofer et al. 2008). For instance, the correlation between detrended March–August SSTs averaged over the region 0°–15°S, 110°–150°E and detrended March–August rainfall averaged over Australia south of 30°S is 0.60 using data from 1958 to 2007 (Nicholls 2010). Interannual variations in SSTs in this region are also closely related to variations in tropical cyclone activity in the Australian region (Nicholls 1984c; Ramsay et al. 2008). The strength of these relationships implies that the reliability of projections of future Australian climate change may be compromised if such projections are made using models unable to accurately simulate and project changes in north Australian SSTs.

Sea surface temperature variations around northern Australia are also closely related to the El Niño–Southern Oscillation (ENSO) phenomenon (e.g., Nicholls 1984b), implying that accurate simulation of ENSO and its links to northern Australian SST are likely prerequisites for reliable projections of Australian climate change. The relationship between north Australian SSTs and indices of ENSO exhibits a strong seasonal cycle, and reproduction of this seasonal variation provides a stringent test of the quality of climate model simulations relevant for projections of Australian climate change. It is worth noting

Corresponding author address: Jennifer Catto, School of Geography and Environmental Science, Monash University, Wellington Road, Clayton VIC 3800, Australia.
E-mail: jennifer.catto@monash.edu

DOI: 10.1175/JCLI-D-11-00311.1

that the correlations mentioned do not necessarily imply direct causal links between the north Australian SSTs and the climate of Australia; nevertheless, the statistical relationships are strong, and the clear links between the north Australian SSTs and the Niño-3.4 SSTs (and between the north Australian SSTs and rainfall) means that projections from models that adequately reproduce these links may be more reliable.

Previous studies have examined the ability of the recent generation of climate models to simulate ENSO in terms of, for example, the spatial pattern of SST anomalies and power spectrum of ENSO-related variance (AchutaRao and Sperber 2002, 2006; Guilyardi et al. 2004; Min et al. 2005; Leloup et al. 2008; Neale et al. 2008; Kug et al. 2010), teleconnections between ENSO and rainfall or mean sea level pressure (e.g., AchutaRao and Sperber 2006), feedback mechanisms (van Oldenborgh et al. 2005; Lloyd et al. 2009, 2010), seasonal cycle (Guilyardi 2006), and decadal variability (Power et al. 2006; Wang et al. 2009). Many of these studies identified similar shortcomings, such as too little variability or too short a period of ENSO, or the maximum variability shifted westward over the tropical Pacific. However, for the Australian region, the connection between north Australian SSTs and ENSO is a vital teleconnection that, as yet, has not been fully explored. We examine in this paper how the global coupled climate models participating in the World Climate Research Programme's (WCRP's) Coupled Model Intercomparison Project phase 3 (CMIP3; Meehl et al. 2000) and assessed for the Intergovernmental Panel on Climate Change (IPCC) Fourth Assessment Report (AR4) reproduce the observed seasonal variation in the relationships between north Australian SST and equatorial Pacific SST indices of ENSO.

The aspect of ENSO simulations we focus on here has special relevance to the Australian climate, but it may also be relevant for more general studies and projections of ENSO. If a model does not reproduce the very strong and seasonally varying relationships between north Australian SSTs and various indices of ENSO, then one may have cause to doubt the credibility of the projections of that model (at least model projections of ENSO behavior, or of climate variations related to ENSO).

Section 2 details the observationally constrained datasets and the models used in the study. The observed relationships between northern Australian SSTs and the Niño-3.4 index of ENSO (SST averaged over the region 5°N–5°S, 170°–120°W) are presented in section 3, followed by an examination of how well the CMIP3 models reproduce these relationships in section 4. We then perform an examination of whether twenty-first-century projections from those models that successfully reproduce the observed relationships suggest changes in these relationships in the future (section 5). Such changes might indicate a possible future change in the nature of ENSO and its links to Australian climate. Section 6 provides a summary and discussion.

2. Data and methods

a. Observational datasets

Two observationally constrained SST datasets have been used to calculate the SST indices used in this study. These are the Met Office Hadley Centre Sea Ice and Sea Surface Temperature (HadISST) dataset (Rayner et al. 2003) and the National Oceanic and Atmospheric Administration (NOAA) Extended Reconstructed SST version 3 (ERSST v3; Smith et al. 2008; Xue et al. 2003) dataset. Data from 1950 to 1999 have been used to document the relationships between ENSO and north Australian SSTs. The two datasets are used to check the consistency of the results. It was found that the results using both datasets agree very well. Therefore, in most of the figures, in the interest of clarity, only the HadISST data are shown.

b. Models

The simulations performed with coupled climate models from various modeling groups around the world for CMIP3, which were utilized in the IPCC AR4, are available from the Program for Climate Model Diagnosis and Intercomparison (PCMDI) data archives. The details of these models are summarized in Randall et al. (2007, their Table 8.1). In this study the twentieth-century simulations, from 1950 to 1999, are used to evaluate the models' ability to represent various aspects of the temporal evolution of tropical SSTs. Where more than one run was performed with the models, only one run, chosen randomly, was used.

One of the transient climate change simulations from the Special Report on Emissions Scenarios (SRES) (Nakićenović and Swart 2000) used in the CMIP3 has also been analyzed for the models from which it is available. The A2 scenario has been chosen as it provides a large CO_2 forcing, increasing from 367 in 2000 to 836 ppm by 2100. This scenario has previously been used to examine many aspects of projected climate change (e.g., Lu et al. 2007, 2008; Alexander and Arblaster 2009; Zhang et al. 2010). The last 50 yr of the twenty-first-century simulations using this emissions scenario have been used so as to have a comparable sample size with the twentieth-century simulations and the observations.

The models investigated in this study are listed in Table 1. These models differ in their atmosphere and ocean resolutions. Previous studies have used regridding

TABLE 1. Models used in this study. Details of the models can be found in Randall et al. (2007).

Identifier	Model
A) BCCR BCM2.0	Bjerknes Centre for Climate Research Bergen Climate Model version 2, Norway
B) CGCM3.1	Canadian Centre for Climate Modelling and Analysis (CCCma) Coupled General General Circulation Model, version 3.1, Canada
C) CNRM	Centre National de Recherches Météorologiques, France
D) CSIRO Mk3.0	Commonwealth Scientific and Industrial Research Organization Mark version 3.0, Australia
E) GFDL CM2.0	Geophysical Fluid Dynamics Laboratory Climate Model version 2.0, United States
F) GISS-AOM	Goddard Institute for Space Studies Model, version E3 coupled with Russell ocean model, United States
G) GISS-EH	Goddard Institute for Space Studies Model, version E3 coupled with Bleck ocean model, United States
H) GISS-ER	Goddard Institute for Space Studies Model, version E3 coupled with Russell ocean model, United States
I) IAP FGOALS	National Key Laboratory of Numerical Modeling for Atmospheric Sciences and Geophysical Fluid Dynamics (LASG)/Institute of Atmospheric Physics Flexible Global Ocean–Atmosphere–Land System Model, China
J) INM-CM3.0	Institute for Numerical Mathematics Coupled Model, version 3.0, Russia
K) IPSL CM4	L'Institut Pierre-Simon Laplace Coupled Model, version 4A, France
L) MIROC3.2(medres)	Model for Interdisciplinary Resarch on Climate 3.2, medium-resolution version, Japan
M) MIROC3.2(hires)	Model for Interdisciplinary Resarch on Climate 3.2, high-resolution version, Japan
N) MIUBECHOG	Meteorological Institute of the University of Bonn, ECHAM + Global Hamburg Ocean Primitive Equation model, Germany/Korea
O) MPI-ECHAM5	Max Planck Institute European Centre Hamburg Model, version 5, Germany
P) MRI CGCM2.3	Meteorological Research Institute Coupled General Circulation Model, version 2.3, Japan
Q) NCAR CCSM3	National Center for Atmospheric Research Community Climate System Model, version 3, United States
R) HadCM3	UK MetOffice Hadley Centre Coupled Climate Model, version 3, United Kingdom
S) HadGEM1	UK Met Office Hadley Centre Global Environmental Model, United Kingdom, version 1

techniques to obtain a common resolution (e.g., Joseph and Nigam 2006); however, in this study the SST indices that are used are calculated as averages over specific regions of the oceans, so no regridding has been performed. The models also differ greatly in their representation of physical processes, details of which can be found in Randall et al. (2007).

c. Analysis method

This study makes use of two commonly used SST indices. Both are calculated using monthly-mean SST values from two observationally constrained datasets (HadISST and ERSST) and from the models. The first region of interest is the Niño-3.4 region, which lies between 5°S and 5°N and between 170° and 120°W. The second region is the north Australian SST region of 0°–15°S and between 110° and 150°E as used in Nicholls (2010).

The two indices were used to examine the composite evolution of the El Niño and La Niña events by identifying events with a simple automated method based on the technique used by the Climate Prediction Center (CPC; http://www.cpc.noaa.gov/products/analysis_monitoring/ensostuff/ensoyears.shtml). First, the trend was removed from the full time series and then the monthly-mean values were removed to produce the SST anomalies. The average SST anomalies for the Niño-3.4 region were calculated for every overlapping 3-month period (e.g., January–March; February–April). A warm (cold) event was defined as having occurred if the 3-monthly mean was greater (less) than or equal to 0.5°C (−0.5°C) for five consecutive 3-month periods (as in CPC) in one year.

Because the focus of this study is on how the SST anomalies develop in the Niño-3.4 and north Australian regions during El Niño and La Niña events, for the events that last more than one year, only the year during which the first development of the event occurred was used in the compositing. A requirement was placed on the events that the Niño-3.4 SST anomaly in January and December of the same year must differ in sign. Years that match the above criteria were then defined as "year 0", with "year −1" being defined as the year before and "year +1" as the year after. The concurrent anomalies for the north Australian region are calculated in the same way.

The method described above identified six El Niño and six La Niña events. They are compared with those

TABLE 2. Years during which there was an observed El Niño or La Niña event (taken from the CPC website) and whether they were identified for compositing by the method described in the text (D), not included due to being a continuation from the previous year (C), or not identified because they were a short, late-developing event (L).

Observed El Niño events	Observed La Niña events
1951 D	1950 C
1957 D	1954 D
1963 D	1955 C
1965 D	1956 C
1968 L	1964 D
1969 C	1967 L
1972 D	1970 D
1976 L	1971 C
1977 C	1973 D
1982 C	1974 C
1986 L	1975 C
1987 C	1988 D
1991 C	1998 D
1994 C	1999 C
1997 D	—

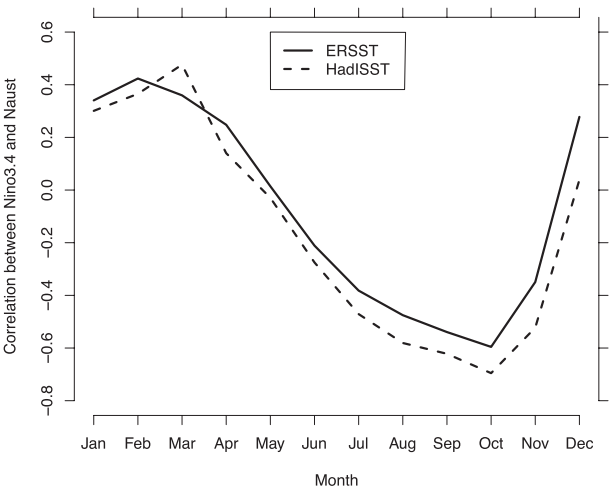

FIG. 1. Monthly correlations between the Niño-3.4 and north Australian SST indices from the ERSST and HadISST datasets, for 1950–99. Correlations are significant at the 95% level for correlations exceeding a magnitude of 0.288.

classified by the CPC in Table 2. Six El Niño events and six La Niña events identified by the CPC method are not included in the events in this study because of their continuation from a previous year. A further two El Niño events and one La Niña event were also not identified by our method because of the development of the event late in the year, meaning there were not five consecutive months with large anomalies of the same sign.

There are numerous ways to identify El Niño and La Niña events using SST anomalies and/or sea level pressure data (e.g., Rasmusson and Carpenter 1982; AchutaRao and Sperber 2002). In this study, the important aspect of the identification procedure is that it is automated and objective, so that the same method can be used on data from a large number of climate model simulations.

3. Observed connection between ENSO and north Australian SST

The seasonal cycle of correlation between the monthly-mean Niño-3.4 index and the monthly-mean north Australian index is shown in Fig. 1 for the HadISST and ERSST datasets detrended by month. For 50 yr of data, the correlations are significant at the 95% level if they are greater (less) than 0.288 (−0.288). From January to April, the correlation between the two indices is positive, with the maximum (which is statistically significant) occurring in either February or March (dependent on the dataset). In other words, at the beginning of the year if there is a warm anomaly in the Niño-3.4 region, on average there is also a warm anomaly in the north Australian region and vice versa. The correlation then changes sign in May and remains strongly negative until November, with the maximum negative correlation occurring in October for both datasets. This means that the anomalies in the two regions are of opposite sign during this period. There is a sharp transition from negative to positive correlations in November.

The seasonal cycle of correlations between the Niño-3.4 and north Australian SST indices can also be demonstrated using the composite evolution of ENSO events, similar to Torrence and Webster (1998). Figure 2 shows this evolution using the HadISST data. The events are identified as described in section 2c, and the composite Niño-3.4 index and corresponding composite north Australian index are plotted along with the one standard deviation range calculated using the nonevent years. This measure of the variability is used to give information about how different the El Niño and La Niña event years are from all the other years.

Looking first at the El Niño evolution, Fig. 2a shows that in the year preceding a warm event (year −1), the Niño-3.4 anomalies are negative but within one standard deviation of the mean. In year 0 the Niño-3.4 anomalies cross the zero line between March and April and then continue to grow, with the average maximum occurring in November or December. These large anomalies during the peak of the El Niño events lie well outside the one standard deviation range shown. The Niño-3.4 anomalies then decrease in the following year, crossing the zero line in June. This pattern is similar to the composite evolution calculated by Torrence and Webster (1998) for all events occurring between 1877 and 1995. The north Australian

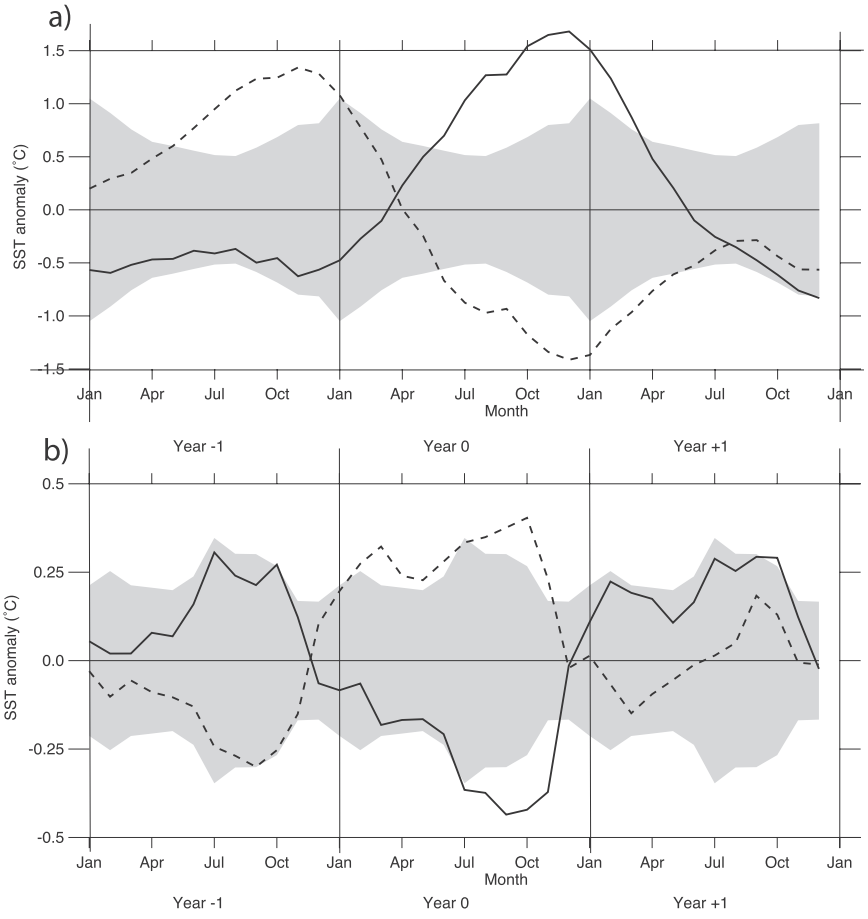

FIG. 2. Composite evolution of the SSTs (°C) for El Niño and La Niña events in HadISST (method described in text) for the (a) Niño-3.4 and (b) north Australian SST indices. Events are listed in Table 2 (indicated by a "D" in the table). Solid lines represent El Niño events, and dashed lines represent La Niña events. Gray shading shows plus and minus one standard deviation calculated using the nonevent years.

SST anomalies associated with the El Niño events (Fig. 2b) begin in year −1 as positive anomalies, corresponding to the negative correlation seen during the months April–November (Fig. 1). Between November and December, the anomalies undergo a swift change of sign from positive to negative. From December to April, the anomalies in the two regions are of the same sign, corresponding to the positive correlation seen in Fig. 1 at the beginning of the year. The cold anomalies in the north Australian region get larger until a maximum of approximately 0.4°C in November. Again, there is a very swift change in the anomaly after November. The largest anomalies—that is, those occurring between July and November—lie outside the one standard deviation range. This shows that although the events are selected according to the Niño-3.4 SST index, the associated anomalies in the north Australian region still lie outside the variability seen during all other years.

The evolution of SSTs associated with La Niña is approximately opposite of that associated with El Niño in both the Niño-3.4 and north Australian SSTs. The temperature anomalies in the development stage (from October year −1 to May year 0) cross the zero line in the same month as for El Niño for both the Niño-3.4 index and the north Australian index. In year +1, the SST anomalies associated with La Niña events in both regions do not return to the values seen in year −1 as they do during El Niño events. This may be because many of the observed La Niña events continue into the next year.

4. Model representation of the ENSO–northern Australian SST relationships

To have confidence in the projections of climate change for Australia, it is important that the seasonal cycle of SST covariations between the Niño-3.4 region

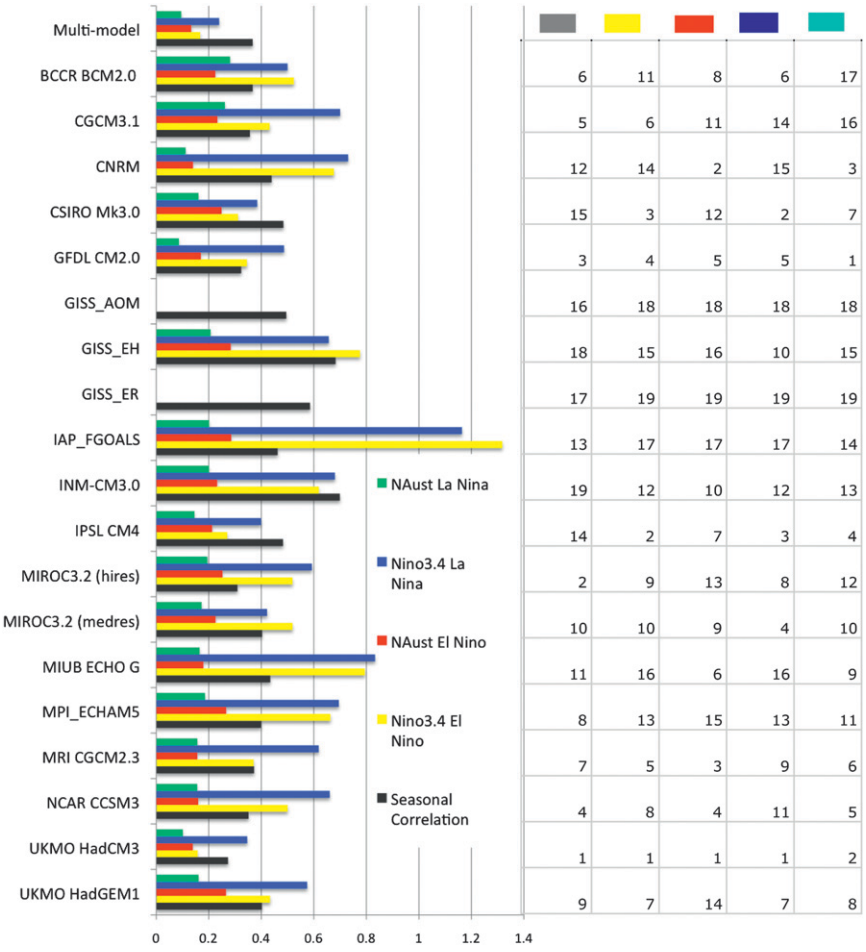

FIG. 3. RMSE for the correlations between Niño-3.4 and northern Australia indices, composite evolution of Niño-3.4 SSTs during El Niño events, and composite evolution of north Australian SSTs during El Niño events, in each of the models in the twentieth-century simulations (1950–99). Rankings for each of the models and for each of the measures are given on the right-hand side.

and the north Australian region is well represented in current global climate models. In this section the monthly correlations between the Niño-3.4 and north Australian indices and the composite evolution of El Niño and La Niña events from the models are evaluated against those presented from the observationally constrained datasets in section 3. First, an overview of the models' performance in all of the measures is given, followed by a more detailed discussion of the seasonal correlations, and the composite ENSO evolution.

a. Overview of model performance

The root-mean-square error (RMSE) of the monthly correlation coefficients, and of the 3-yr SST anomaly evolution during warm and cold events, are shown in Fig. 3. The RMSE is calculated using the following equation:

$$\mathrm{RMSE} = \sqrt{\frac{1}{N}\sum_{i=1}^{N}(x_{m.i} - x_{o.i})^2}, \qquad (1)$$

where $N = 12$ for the monthly correlations and $N = 36$ for the composite evolutions, x_m is the value of interest from the model, and x_o is the value from HadISST. The ranks of each model for each measure are also given in Fig. 3, ranking the model with the lowest RMSE for a particular measure as number one. One noticeable feature of Fig. 3 is the large range in RMSE values across the models.

Some of the models seem to be able to capture one or two of the measures quite well, but they are ranked lowly for the other measures. For example, CSIRO Mk3.0 (full model names are given in Table 1) is ranked

second for the north Australian index during El Niño events, but it is ranked at 3, 12, 14, and 15 for the other measures. However, there are other models that perform very well for all of the measures (e.g., HadCM3) or that perform very badly for all of the measures (e.g., GISS-AOM). This has been analyzed in more detail by investigating the links between the RMSE for the different measures. An assessment of the RMSE for the composite event evolution of Niño-3.4 and north Australian SSTs shows some interesting links between the representation of the two regions in the models. First, for the Niño-3.4 regions, there is a correlation between the RMSE values for El Niño and La Niña events of 0.91. This means that if the model can capture the Niño-3.4 evolution in an El Niño event, then it likely can during a La Niña event. The correlation between events for the north Australian region is 0.65, which is also relatively high (and significant at 95%). The correlation for the RMSE from the models between the Niño-3.4 and north Australian regions during El Niño is 0.51, and during La Niña it is 0.38. If the correlation between the ranks of the models for each measure (shown in Fig. 3) is considered, then the link between the abilities of the models to capture the SSTs of the two regions during El Niño events is 0.58 and for La Niña events it is 0.56. This suggests that the better a model performs in representing the Niño-3.4 SST evolution, the better it is likely to be in representing the north Australian SST evolution during both El Niño and La Niña events.

b. Seasonal cycle of correlations

From Fig. 3, and as discussed in the previous section, there is a large spread in the values of RMSE of seasonally varying correlations between the Niño-3.4 and north Australian SSTs for the models. The 19 models have been separated into three groups according to their performance for this measure, judged by the RMSE. Figure 4 shows the monthly correlations between the detrended Niño-3.4 and north Australian indices for the models listed in Table 1 grouped by RMSE performance, along with the detrended HadISST monthly correlations (also seen in Fig. 1), and the multimodel mean for all models. The RMSE that has been used to group the models is the sum of both the bias and the centered pattern RMSE, which depends on the variance of the observations, the model, and the correlation coefficient between the observations and the model (Taylor 2001). To help with the interpretation of Fig. 4, Fig. 5 shows a Taylor diagram for each of the 19 models, and for the ERSST dataset for the monthly correlations between Niño-3.4 and north Australian SSTs. The letters represent the different models and the size of the symbol represents the bias, with the larger symbol representing smaller bias and the smaller symbol representing higher bias. The Taylor diagram can be used, along with the total RMSE, to assess the ability of the models to represent the monthly correlations in terms of bias, correlation coefficient, and variance. The point showing the ERSST data provides an indication of the best result that could be expected from a near-perfect model, since it compares two observational datasets. Some models do quite well in comparison with this difference between the two observational datasets.

The multimodel mean seasonal correlations are shown in Fig. 4 and show a reasonable cycle with positive correlations at the beginning of the year and negative correlations from June to November, although the shift from positive to negative occurs too late. The magnitudes of the multimodel mean correlations are too small, with the largest correlation being about 0.2. The six models with the lowest total RMSE for the monthly correlations are HadCM3, MIROC3.2(hires), GFDL CM2.0, NCAR CCSM3, CGCM3.1, and BCCR BCM2.0, and these are shown in Fig. 4a. Of these, the model that performs best in representing the seasonal cycle of correlations is HadCM3 (Fig. 4a). This model has been shown in previous studies to perform well in representing ENSO variability, in particular the seasonal cycle of tropical Pacific SST variance (Joseph and Nigam 2006). In the Taylor diagram (Fig. 5), HadCM3 shows a standard deviation that is very close to the observations, and the mean bias is small. This model has a lower correlation with the observations than some of the other models, which is due to the maximum and minimum values occurring a month later than in the observations (Fig. 4a).

The seasonal cycle of correlations is also well represented in GFDL CM2.0, which was shown to capture the seasonality of ENSO SST variance in previous studies (Wittenberg et al. 2006). In the current study, it has been found that it also represents the seasonal cycle of north Australian SST variance well (although the magnitude of the variance is too high; not shown), leading to the very good seasonal cycle of correlation between the two series of SST anomalies. The Taylor diagram in Fig. 5 shows that GFDL CM2.0 has a standard deviation quite a bit higher than the observations and a larger mean bias than HadCM3 due to the slight positive shift in the monthly correlations, but the correlation between the model and the observations is good.

MIROC3.2(hires) has a lower total RMSE than the corresponding medium resolution model, despite having a lower correlation with the observations, and also a lower standard deviation (Fig. 5). The improvement in total RMSE can therefore be ascribed to a lower bias. MIROC3.2(hires) has previously been shown to have low variability in the tropical Pacific (Joseph and Nigam

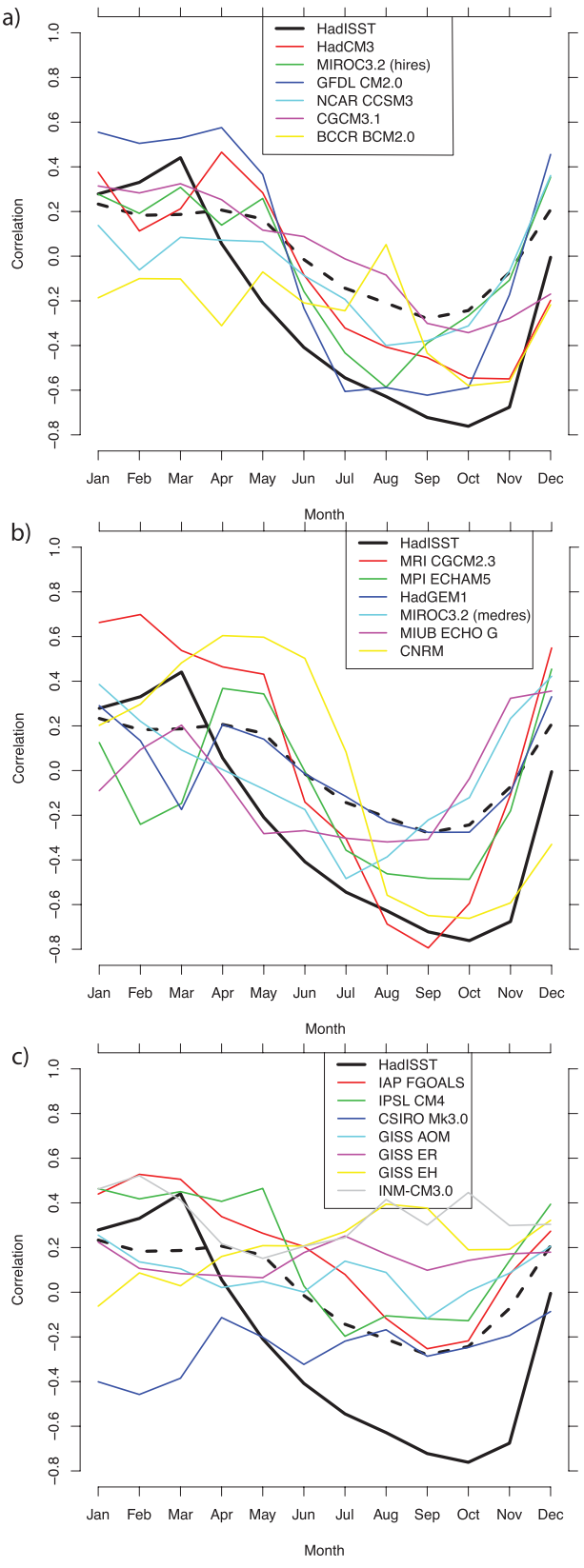

2006). As in MIROC3.2(medres), the lowest monthly correlation between the Niño-3.4 and north Australian SSTs occurs too early in the year [August for MIROC3.2(hires) and July for MIROC3.2(medres)].

NCAR CCSM3 has previously been shown to capture the seasonal phase locking of the Niño-3.4 index (Joseph and Nigam 2006; Neale et al. 2008). In Fig. 4a the correlation between the Niño-3.4 and north Australian indices shows a weak seasonal cycle that can also be seen in the Taylor diagram (Fig. 5). This suggests that although the seasonal cycle of Niño-3.4 is well represented, the seasonal cycle of the model's north Australian index is weak and the links between the SST anomalies in the two regions are not as well simulated as some of the other models. The small total RMSE appears to be mainly due to a small bias.

Despite having low values of RMSE, CGCM3.1, and BCCR BCM2.0 do not show a strong enough seasonal cycle and have standard deviations much lower than the observations (Fig. 5). The seasonal cycle of correlations in BCCR BCM2.0 has a small bias but a poor correlation with the observations, while CGCM3.1 has a high correlation with the observations but a very large bias. These two models highlight very well the problem with judging model performance by only looking at the total RMSE, as they fall into the group with the lowest RMSE values, but they clearly have problems in representing the observed seasonal pattern.

Figure 4b shows the seasonal cycle of correlations for the models with intermediate values of total RMSE. Some of the models in this group subjectively appear to be doing as well as those in the best group at capturing the seasonal cycle of correlations, but they have been placed in this middle group objectively by using the values of the RMSE. It can be seen that CNRM represents the minimum negative monthly correlations toward the end of the year quite well. In the Taylor diagram, this model shows almost the same standard deviation as the observations. The large discrepancy in the middle of the year, however, results in quite a large total RMSE for this model, partially due to a bias and partially to a low correlation with the observations. The

←

FIG. 4. Monthly correlations between the Niño-3.4 and north Australian SST indices for detrended HadISST and the IPCC AR4 models: (a) the six models with the lowest RMSE values, (b) the six models with medium-range values of RMSE, and (c) the seven models with highest RMSE for the correlations. Thick black dashed line shows the multimodel mean seasonal correlation. Correlations are significant at the 95% level for correlations exceeding a magnitude of 0.288.

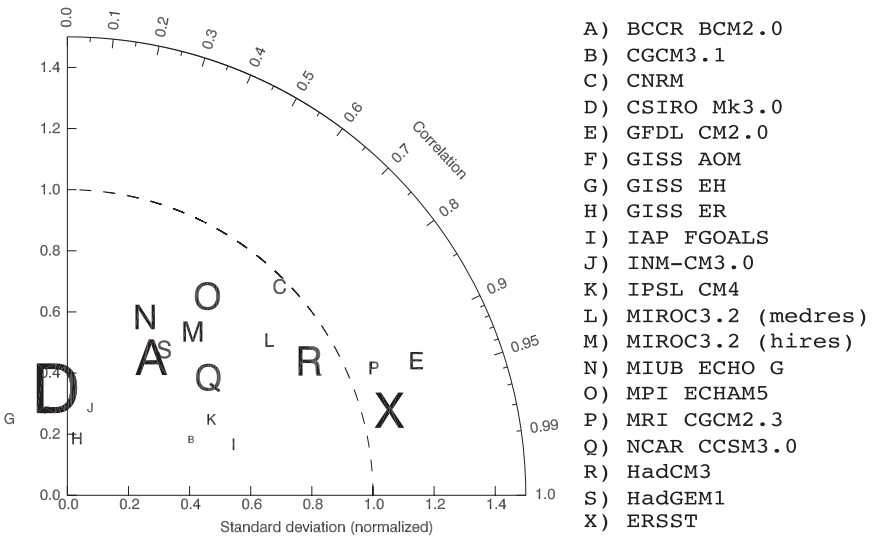

FIG. 5. Taylor diagram for the seasonal correlation between Niño-3.4 and north Australian SSTs. Each model is represented by a letter given in the figure. Bottom-left corner of the letter is the point on the diagram. "X" represents the ERSST dataset. Size of the symbol is inversely proportional to the bias.

other models in this group with similar characteristics are MRI CGCM2.3 (which actually has a higher standard deviation than the observations) and MIROC3.2(medres). These two models correlate more strongly with the observations than CNRM (Fig. 5). HadGEM1, MPI-ECHAM5, and MIUBECHOG have too weak a seasonal cycle and have some problems with timing and erroneous negative monthly correlations at the beginning of the year (Fig. 4b). These three models (S, O, and N, respectively, in the Taylor diagram in Fig. 5) therefore have poor correlations with the observed cycle and large biases.

Figure 4c shows the models with the highest RMSE values for the monthly correlations. INM-CM3.0, GISS-ER, GISS-EH, and GISS-AOM have monthly correlations that are almost always positive and do not vary greatly over the year. In the Taylor diagram in Fig. 5, the models in the group with highest RMSE values for the monthly correlations lie very close to zero in terms of their normalized standard deviations and correlation coefficients between model and observations, and most models show a large bias. In CSIRO Mk3.0, the monthly correlations are negative throughout the year (Fig. 4a), resulting in the fifth largest RMSE (0.484). In the Taylor diagram, this model shows that both the normalized standard deviation and the correlation coefficient with observations are close to zero, but the model shows a very small bias (because of compensating biases at different times of the year). IPSL CM4 and IAP FGOALS show a reasonable seasonal cycle of monthly correlations; however, the negative correlations toward the end of the year are far too weak. This gives a total RMSE for both models that is quite high, but as can be seen in the Taylor diagram, this is due to the smaller-than-observed variance and large bias, rather than poor correlation between the model and observations.

c. *Composite ENSO evolution*

The El Niño and La Niña events were identified in each model using the same method as for the observations, described in section 2c. The number of events found is given in Table 3 for the observations and each model for both the twentieth-century and twenty-first-century simulations (for the models for which the data were available). As discussed above, in the 50 yr of HadISST data used, six El Niño and six La Niña events were identified. In some of the models, very few events are identified (e.g., CGCM3.1, BCCR BCM2.0, and the MIROC models), which will make the composite evolution of SST anomalies particularly noisy. For two of the models (GISS-ER and GISS-AOM), the tropical Pacific SST variability was so small that no events were identified in the twentieth-century simulations.

Figures 6 and 7 show the composite evolution of the twentieth-century model-simulated Niño-3.4 SST anomalies (Figs. 6a and 6c, and Figs. 7a and 7c) and the north Australian SST anomalies (Figs. 6b and 6d, and Figs. 7a and 7c) for the El Niño events and La Niña events,

TABLE 3. Number of El Niño events and La Niña events detected in each of the models in the twentieth-century simulations (1950–99) and the twenty-first-century simulations of SRES A2 (2050–99; a dash indicates these data are not available).

	Twentieth century		Twenty-first century	
Model	El Niño	La Niña	El Niño	La Niña
HadISST	6	6	—	—
BCCR BCM2.0	2	2	—	—
CGCM3.1	1	1	2	5
CNRM	7	10	9	7
CSIRO Mk3.0	7	9	4	8
GFDL CM2.0	4	12	4	8
GISS-ER	0	0	0	0
GISS-EH	3	3	—	—
GISS-AOM	0	0	—	—
IAP FGOALS	5	11	—	—
INM-CM3.0	5	9	6	8
IPSL CM4	9	10	—	—
MIROC3.2 (medres)	2	3	0	0
MIROC3.2(hires)	3	2	—	—
MIUBECHOG	13	12	9	10
MPI-ECHAM5	5	6	7	7
MRI CGCM2.3	6	6	9	10
NCAR CCSM3.0	10	11	3	3
HadCM3	5	6	4	4
HadGEM1	2	4	7	6

respectively. For the plotting, the models have been kept in the same groups as in Fig. 4, and only the top two groups are being shown in Figs. 6 and 7. Because of the method of selecting the events according to a particular pattern of Niño-3.4 SST evolution, it should be expected that the patterns seen in the models would show a good representation of the evolution of the Niño-3.4 index. However, the evolution of the north Australian SSTs is not directly constrained by the method of selection of the events and so might be expected to show more variation. Again, to aid interpretation, Figs. 8a and 8b show the Taylor diagrams for the El Niño and La Niña events, respectively, for the top two groups of models.

Looking first at the general picture of the El Niño events (Figs. 6a and 6c), it can be seen that many of the models show a reasonable representation of the SST evolution in the Niño-3.4 region. The timing of the development of the warm anomaly is captured well, and some of the models' anomalies (NCAR CCSM3, HadCM3, GFDL CM2.0, CGCM3.1, MPI-ECHAM5, HadGEM1) reach magnitudes similar to that of the HadISST anomaly. There is a larger spread in the models' abilities to represent the north Australian SST anomaly evolution (Figs. 6b and 6d), but some of the models are able to capture the timing of the swift change of sign of the anomaly in October or November (e.g., HadCM3, MPI-ECHAM5, MRI CGCM2.3, CNRM). The Taylor diagram in Fig. 8a shows that for the Niño-3.4 index, there is generally a high correlation with the observations but also quite a large spread in the standard deviation. The correlation with observations is generally lower for the north Australian SSTs, and there is also a large spread in the standard deviation for this measure.

Figures 6a and 6b show that HadCM3, which has the lowest RMSE for both the Niño-3.4 and north Australian SST indices during El Niño events, represents the timing of the development and also the magnitude of the SST anomalies in both regions very well. The Taylor diagram in Fig. 8a shows that HadCM3 has standard deviations for both indices that are very close to the observed values, and that have very high correlations with the observations and a very small bias. MIROC3.2(hires), despite being ranked very highly for the seasonal cycle of correlations, shows quite low variability in the Niño-3.4 region (Fig. 6a), with the SST anomalies not reaching the magnitude of the observed anomalies. This is also clearly shown in the Taylor diagram (Fig. 8a). GFDL CM2.0 shows an evolution of the Niño-3.4 index that begins well and then reaches almost to the magnitude of the observed positive anomaly, and that after decaying it has a negative anomaly that is too strong. In the Taylor diagram in Fig. 8a, this model appears to be quite successful in representing the Niño-3.4 evolution, with a small bias, a good correlation with the observations, but with a standard deviation higher than that observed. The north Australian SSTs during El Niño in GFDL CM2.0 are also quite well represented, compared to other models, but they have a variance that is higher than the observations. NCAR CCSM3 shows a distinctly semiannual evolution, with the Niño-3.4 SST anomalies being positive at the beginning of year −1 in the El Niño events and negative in the La Niña events (Fig. 6a), resulting in this model having a high number of identified events (Table 3). This is a well-known feature of the NCAR CCSM3 model (Neale et al. 2008), and it can also be seen in MIUBECHOG in Fig. 6c. NCAR CCSM3, despite having a low RMSE for the north Australian index, does not capture the magnitude of the SST anomalies in this region in either warm or cold events. Its very low variance in the north Australian region during both El Niño and La Niña events can be clearly seen in the Taylor diagrams in Figs. 8a and 8b. CGCM3.1 represents the evolution of Niño-3.4 SSTs quite well but with too small a variance (Figs. 6a and 8a). The north Australian SSTs in this model show quite a low correlation with the observations due to the strong negative anomaly during year −1. The SST evolutions in the BCCR BCM2.0 have standard deviations that are much too high in both regions. Both BCCR BCM2.0 and CGCM3.1 have a very low incidence of El Niño and La Niña events, and so the evolution of SSTs shown is very noisy.

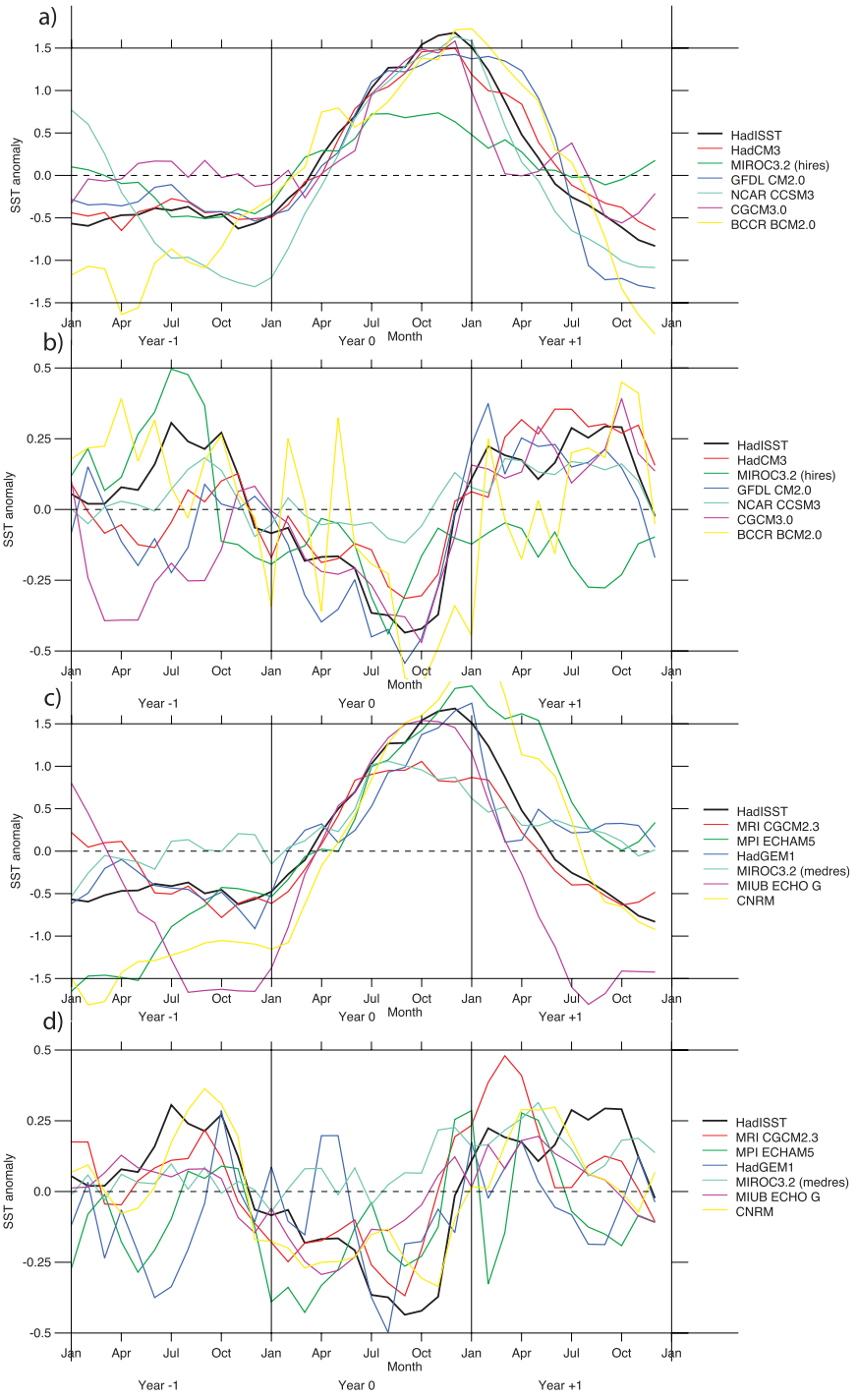

FIG. 6. Composite evolution of the SSTs (°C) for the El Niño events identified in the models (method described in text) for (a),(c) Niño-3.4 and (b),(d) north Australian SST indices. (top two panels) Top group and (bottom two panels) middle group of models according to the RMSE of the seasonal cycle of correlations. Correlations are significant at the 95% level for correlations exceeding a magnitude of 0.288.

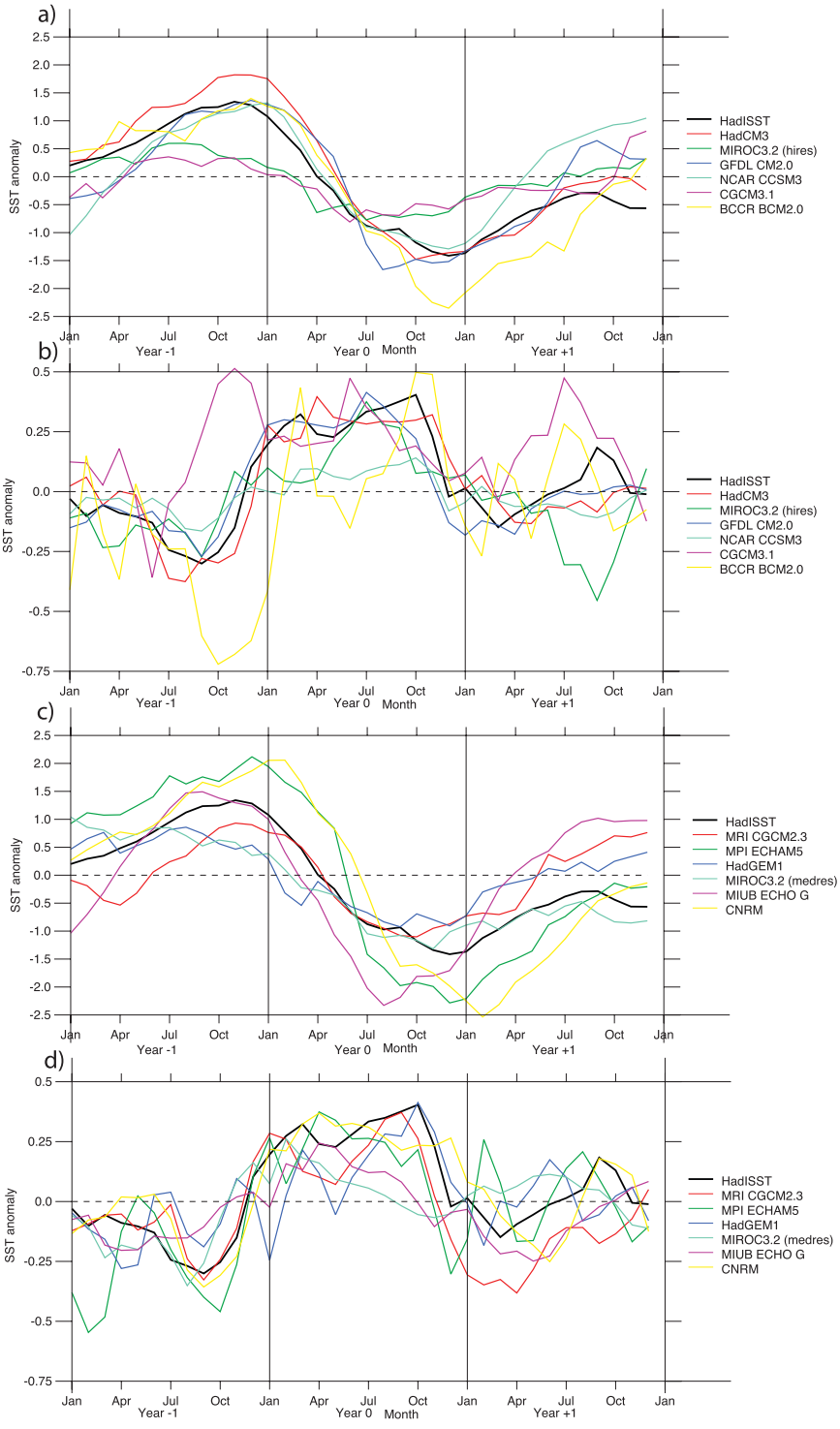

FIG. 7. As in Fig. 6, but for La Niña events.

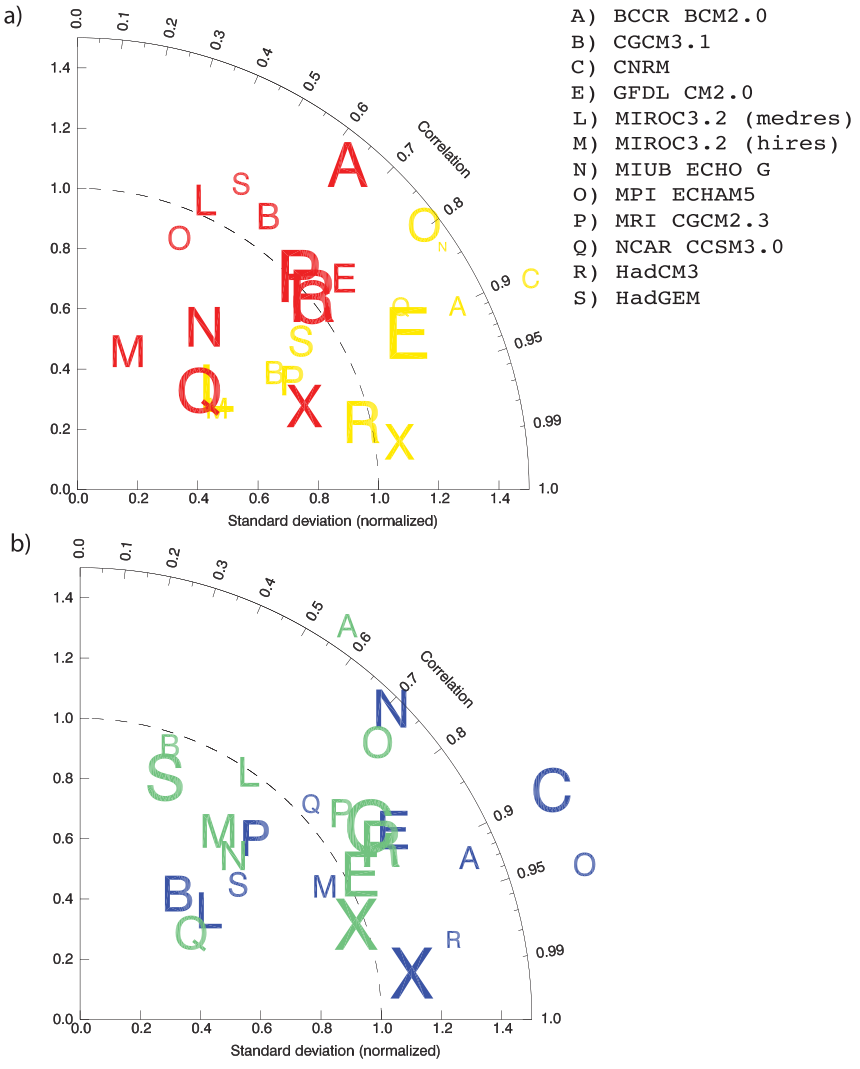

FIG. 8. Taylor diagrams for (a) the evolution of SSTs during El Niño (yellow is Niño-3.4; red is north Australian) and (b) the evolution of SSTs during La Niña (blue is Niño-3.4; aqua is north Australian). "X" represents the ERSST dataset. Bottom-left corner of the letter is the point on the diagram. Size of the symbol is inversely proportional to the bias.

The second group, with higher values of RMSE for the seasonal cycle of correlations, is shown in Figs. 6c and 6d. MRI CGCM2.3 shows a good evolution of SSTs, but the magnitude of the positive anomaly is not large enough, and so on the Taylor diagram it shows a lower standard deviation than the observations. The representation of the north Australian SSTs is very good, and this model is ranked third for this measure. MPI-ECHAM5 is ranked quite low for both the Niño-3.4 and north Australian SST evolution during El Niño and fails to capture the timing of the Niño-3.4 SST evolution and the pattern of the north Australian evolution. HadGEM1 only has two El Niño events identified, and it shows a good representation of the Niño-3.4 SSTs with standard deviations close to those observed and a good correlation with the observations (Fig. 8a), but the north Australian SST evolution is not well captured at all. MIROC3.2(medres) exhibits low SST variability in the tropical Pacific (not shown), and consequently only few events are identified in this model. It can be seen in Fig. 6c that this model fails to capture the evolution of Niño-3.4 and north Australian SSTs during El Niño events, and this is confirmed by its position in the Taylor diagram (Fig. 8a) with a very low standard deviation and

a correlation with observations for the north Australian SSTs very close to zero. CNRM is ranked second in the representation of north Australian SST evolution during El Niño, which is demonstrated in Fig. 6d. The Taylor diagram shows that the standard deviation of this measure in CNRM is almost exactly that of the observations. However, there is much larger variance in the Niño-3.4 region than observed.

For the La Niña events (Fig. 7), the composite evolution for the Niño-3.4 index is generally not as well captured as for the El Niño events. The models have difficulty simulating the variance and the correct timing of the development of the cold anomalies. This is also evident in the Taylor diagram (Fig. 8b), with the models lying farther from the correct standard deviation. This is an interesting result, which suggests that perhaps more work has been done with the models to try to represent El Niño and less focus has been placed on the La Niña events, or that La Niña events are harder to simulate than El Niño events (Ohba and Nohara 2010). The north Australian SSTs during La Niña, however, seem to be better represented than for the El Niño events in many of the models. This can be seen in the Taylor diagram (Fig. 8b) with many of the models showing a higher correlation with the observations.

HadCM3 is the model that represents the Niño-3.4 index during La Niña events best, and it is ranked second in the representation of the north Australian SSTs during La Niña. The magnitude of the warm anomaly in the Niño-3.4 region during year −1 is too large, however, and this is demonstrated in the Taylor diagram with a standard deviation that is higher than the observed and a relatively large bias compared to other models. In the north Australian region, the swift change in sign of the SST anomaly during November of year −1 is very well captured. GFDL CM2.0 is ranked first for the north Australian SSTs during La Niña, and this model shows excellent timing of the evolution of the SSTs, standard deviation that is very close to the observations, and high correlation with the observations. As mentioned in the discussion of the El Niño events, NCAR CCSM3 does not capture the variability of the SSTs in the north Australian region during either warm or cold events as can be seen in Fig. 8. MIROC3.2(hires) performs similarly for La Niña as it does for El Niño, with too little variance shown in both regions. Despite CGCM3.1 performing well at representing the seasonal cycle of correlations, the representation of Niño-3.4 and north Australian SSTs during La Niña is very poor, showing either very low variance (Niño-3.4) or very low correlation with observations (north Australian). BCCR BCM2.0 also performs poorly for the La Niña events, with a variance in both regions that is much too high.

There are some interesting features in the results from the models in the second group. Both MPI-ECHAM5 and CNRM have the cold anomaly in the Niño-3.4 region developing about 3 months too late. For CNRM, this corresponds to the shift of the seasonal cycle seen in the correlations (Fig. 4). The variance is also much too high in this measure for both MPI-ECHAM5 and CNRM, which can be seen in the Taylor diagram (Fig. 8). The north Australian SSTs are well represented in CNRM, with this model capturing the timing and magnitude of the SST anomalies. In MPI-ECHAM5, the SST anomalies in the north Australian region are very ''noisy,'' which is unusual considering that six La Niña events were identified in this model and that the correlation with the observed north Australian SSTs is very low. The variance shown in both regions by MRI CGCM2.3 is fairly close to the observations, but the apparently shorter event length results in the correlation with observations being poor in the Niño-3.4 region. HadGEM1 performs quite poorly in representing the north Australian SSTs during La Niña events, with a correlation with the observations that is very low (as seen in the Taylor diagram in Fig. 8b). Because this model has a small bias, it is ranked eighth for this measure compared to CGCM3.1, which lies close to HadGEM1 on the Taylor diagram but has a large bias and is ranked 17th. As with MIROC3.2 (hires), MIROC3.2 (medres) has low variability in the Niño-3.4 region, which can be seen in the Taylor diagram in Fig. 8b. The north Australian SSTs have good variability compared to the observations, but the correlation with the observations is low because of the too early decay of the warm anomaly and a return to a warm anomaly by the end of year 0. The cold anomaly in the Niño-3.4 region in MIUBECHOG is too strong and develops too early, and the north Australian SSTs do not show enough variability or manage to capture the swift change from a negative to a positive anomaly during November of year −1.

5. Changes in a warming climate

In this section the projections of twenty-first-century climate using the SRES A2 scenario are investigated in two groups of models: the four models that showed the best performance and the four models that showed the worst performance for the seasonal cycle of correlations for which the A2 SRES scenario data were available, and for which at least one El Niño and La Niña event was identified in the twentieth-century and twenty-first-century simulations. The top group comprises HadCM3, NCAR CCSM3.0, GFDL CM2.0, and CGCM3.1, while the bottom group comprises CSIRO Mk3.0, MIUBECHOG, INM-CM3.0, and CNRM. The differences for both

groups are shown to try to gain some understanding into whether the changes in the future warming scenario are different between the models that perform well and those that do not.

a. Correlations

Figure 9 shows the monthly correlations between the Niño-3.4 and north Australian indices for both the twentieth-century and twenty-first-century simulations, and also the differences for the top four models and the bottom four models. The range of differences for both groups of models is centered on zero, with the multimodel mean differences staying very close to zero throughout the year. This suggests that the correlations will not change very much in the future, and that even for the models that represent the link between the regions well, there is very little change.

In HadCM3, which showed the best representation of the seasonal correlation, the change is negative from April to November and slightly positive from December to March. This suggests a slight strengthening of the seasonal cycle of correlations in most months apart from April and May. For GFDL CM2.0, the change in the correlation changes from 0.2 in January to −0.1 in June and back to 0.2 by December. This has very little impact on the seasonal cycle, other than to increase the positive correlation from December to May. NCAR CCSM3 shows changes very close to zero throughout the year, suggesting very little change in the connection between the tropical Pacific and the north Australian region in this model. CGCM3.1 has a negative change for most of the year until September, which means there is a negative correlation for almost the entire year in the twenty-first-century simulation.

In the bottom group of models, the patterns of the seasonal cycle of correlation are very different between the models. Still, the changes in the correlation in all of the models are small, and the multimodel mean difference is close to zero throughout the year. For CNRM, the annual cycle in the twenty-first century is slightly different to the twentieth century. Whereas in the twentieth century, the change from positive to negative correlations occurred very quickly between June and August; in the twenty-first-century simulations, it is a more gradual change, beginning in May and with a minimum in October. The maximum and minimum values of the correlations are very similar. This model suggests that there may be something different occurring in the seasonal cycle to affect the changes in the timing of the change in correlations. The seasonal cycle of correlations in the other models in this group are completely different from those seen with HadISST, and the changes are quite small.

b. Composite evolution

Previous studies have investigated whether the tropical Pacific is likely to move toward more El Niño– or La Niña–like conditions with global warming (e.g., Collins et al. 2005). Table 3 shows the number of events identified in the twentieth-century and twenty-first-century simulations. On average, for all of the models for which the SRES A2 scenario data were available, there is an increase in the number of El Niño events of 0.2 and a decrease in the number of La Niña events of 0.5. Taking the top four models, there is a decrease in El Niño events of 2 and a decrease in La Niña events of 3.25 over 50 yr. This suggests a decrease in tropical Pacific variability generally, rather than a shift from one type of event to another. However, given the small sample, it is not possible to draw any strong conclusions on whether there is any projected change in the frequency of one type of event or another.

Although the correlations between the two regions of interest do not appear to change much in the SRES A2 scenario, the composite evolution of warm and cold events do show some apparent differences. The multimodel mean SST evolutions for the two groups of models shown in the previous section are given in Fig. 10. Figures 10a and 10b show the Niño-3.4 index. During year −1 and year 0, the changes are generally small for both El Niño and La Niña events and for both groups of models. The largest changes in the Niño-3.4 region occur toward the end of year +1, with an increase in SSTs in the year following El Niño events and a decrease in SSTs in the year following La Niña events. In the north Australian SSTs, there is a positive change in the SST anomalies during year −1 and year 0 for the top group of models. The north Australian SSTs during La Niña events show smaller changes, but they generally show a negative difference between the twenty-first-century and the twentieth-century simulations. Most of the changes seen are fairly small relative to the variability between the identified events.

6. Conclusions and discussion

In this study, the connection between ENSO and north Australian SSTs has been investigated in terms of the observations, model representation, and future projections. This is a demanding test of a climate model's ability to simulate climate variations, since the observed relationships between ENSO and north Australian SSTs, although strong, exhibit a complicated seasonal variation. There seems no way in which a climate model could, a priori, be tuned to reproduce these observed relationships (especially since these observed relationships are not well known nor are their causes understood). The key findings are as follows:

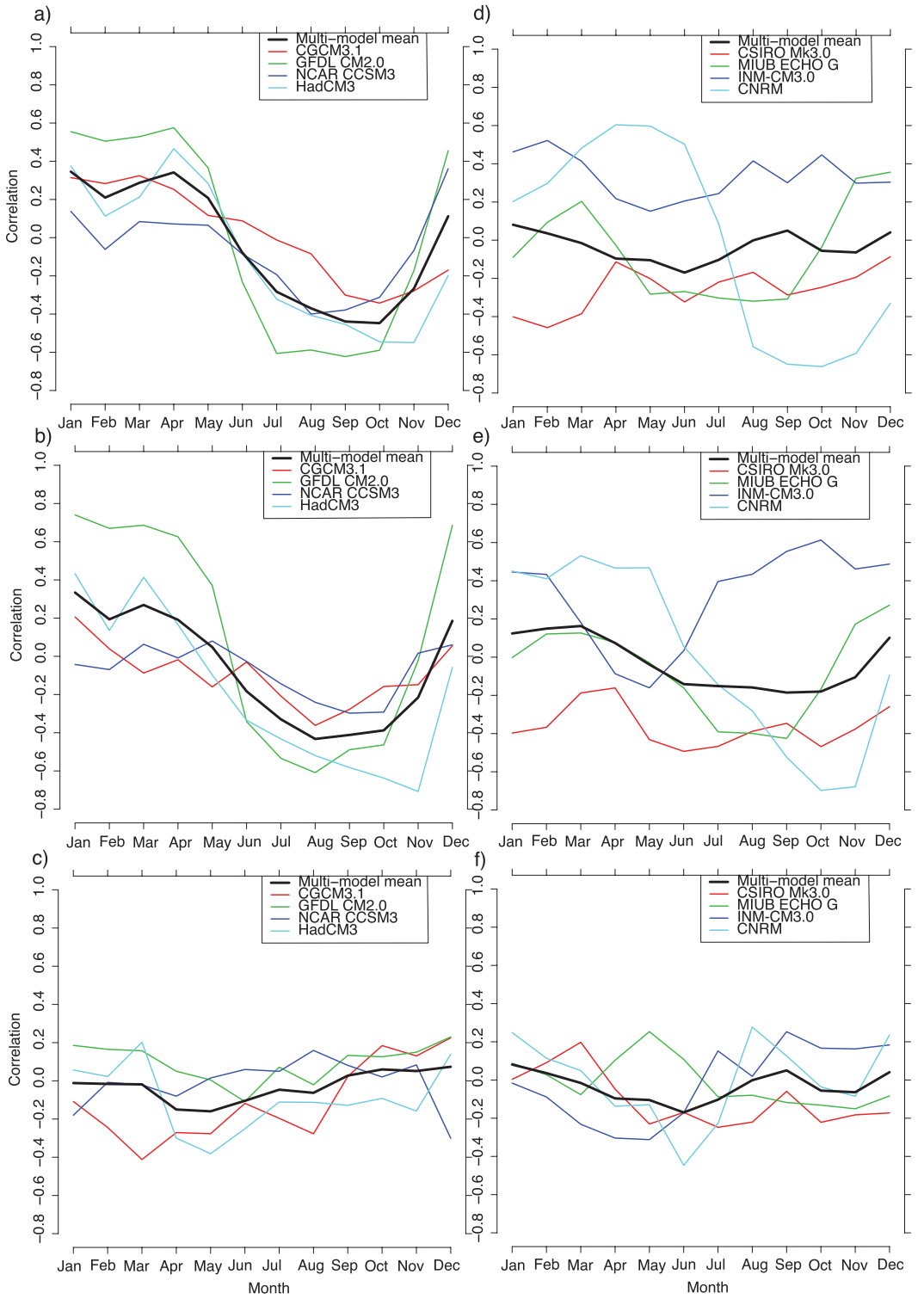

FIG. 9. Monthly correlations between Niño-3.4 and north Australian SST indices from the (top) twentieth century and (middle) twenty-first century (SRES A2) for the (a),(b) top group and (d),(e) bottom group. Differences between the twenty-first century and twentieth century for the (c) top group and (f) bottom group. Correlations are significant at the 95% level for correlations exceeding a magnitude of 0.288.

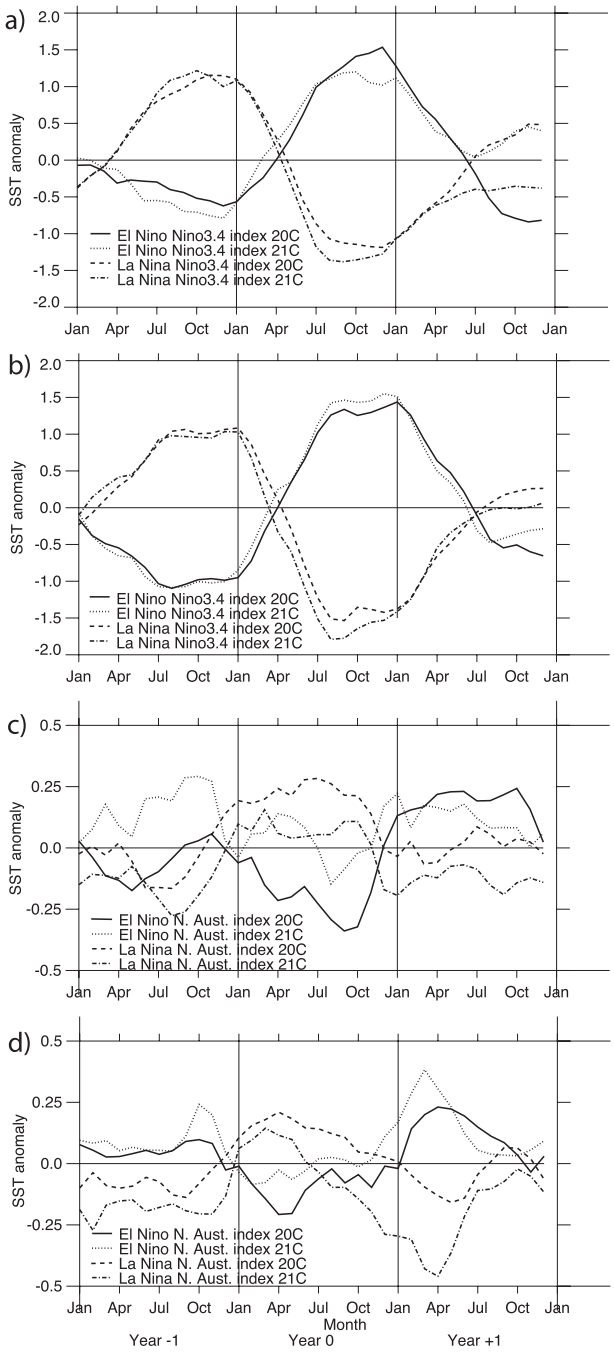

FIG. 10. Multimodel mean SST anomalies for (a),(c) the top four models (according to the seasonal correlation RMSE) and (b),(d) the bottom four models, for the twentieth-century and twenty-first-century simulations, for (top two panels) Niño-3.4 SSTs and (bottom two panels) north Australian SSTs.

- The two observationally constrained SST datasets studied indicate a seasonal cycle of correlation between the tropical Pacific and north Australian SSTs, which is positive from January to April and negative from April to December with a maximum correlation in February or March and a minimum in October.
- There is a large spread in the ability of the CMIP3 climate models to represent the observed seasonal correlation. The six models with the lowest values of RMSE in this measure are HadCM3, MIROC3.2(hires), GFDL CM2.0, NCAR CCSM3, CGCM3.1, and BCCR BCM2.0.
- Some of the models do quite a good job of representing the Niño-3.4 index during El Niño and La Niña events, although there is a large amount of variability in the number of events identified in the different models.
- There is a very large spread in the models' ability to represent the north Australian SST evolution during ENSO events.
- The results from the SRES A2 scenario for the CMIP3 models show a spread in the change to the seasonal cycle, but the multimodel average indicates very little or no change to the seasonal cycle of the correlation between Niño-3.4 and north Australian SSTs.
- For the evolution of individual ENSO events, the multimodel average shows a possible earlier development of La Niña cold anomalies in the Niño-3.4 region and a weakening of the north Australian SST anomalies associated with the events in the twenty-first-century simulations.

These results indicate that although the Niño-3.4 SST evolution is well represented in most models, this does not necessarily mean that the simultaneous north Australian SSTs will also be well represented. Many of the models have difficulties capturing the covarying nature of the two regions, which has impacts on the ability of the climate models to credibly represent current and very likely future Australian climate. However, there is a link between the ability of a model to represent the Niño-3.4 SSTs and the north Australian SSTs, as discussed in section 4b.

Some of the models, which have been shown in this study to perform well at representing the link between the Niño-3.4 and north Australian regions, have previously been shown to represent other aspects of ENSO variability well. For example, HadCM3 has a good representation of the ENSO power spectrum and the seasonal cycle of variability (e.g., Joseph and Nigam 2006; van Oldenborgh et al. 2005). A common feature of climate models is the anomalous westward extension of ENSO variability into the Maritime Continent (e.g., Joseph and Nigam 2006; Kug et al. 2010), which could be a factor in some of the models being unable to simulate

the negative correlations between the two regions of interest during the latter part of the year.

There are many possible aspects of the simulations that could be responsible for the spread in the representation of the seasonal cycle of covariation of the SSTs. These could be ocean related or have to do with the large-scale atmospheric circulation. The models that perform well have a range of resolutions, suggesting that this is not the major factor, although Roberts et al. (2009) show that a higher ocean and atmosphere horizontal resolution leads to better ENSO representation. The possibility that models with and without flux corrections could give different results was also investigated, and it was found that the models that do use flux corrections were spread throughout the results from the models, suggesting that this is not an important factor for the representation of the links discussed in this study. The variation between the models could also be the result of atmosphere feedbacks (Lloyd et al. 2009) and the representation of deep convection (e.g., Neale et al. 2008; Guilyardi et al. 2009). The physical processes that link the SST anomalies of the two regions and why some models represent them well and others do not will be the subject of a future study.

The future climate of the tropical Pacific region has been the subject of much recent research. Some climate models forced with increased greenhouse gases show an enhancement of the warming signal in the tropical SSTs and a weakening of the Walker circulation (Held and Soden 2006). This has been described in the literature as ''El Niño like''; however, DiNezio et al. (2010) show that this is a confusing analogy because of the large differences between anomalous conditions during El Niño and the changes seen with greenhouse warming, for example, the differences in the behavior of the Hadley circulation. Collins et al. (2005) find that there is not a preference for the tropical Pacific to become more El Niño like or more La Niña like with enhanced greenhouse warming.

Of the models found in this study to best represent the seasonally covarying nature of ENSO and north Australian SSTs, some show an increase in El Niño events and some show an increase in La Niña events with increased greenhouse emissions, somewhat consistent with Collins et al. (2005). The changes to the evolution of the ENSO events seen in the A2 scenario simulations come from quite a small sample of events, and therefore no strong conclusions can be drawn about the impact that such changes might have on the system. There are indications from this study that the SST anomalies in the tropical Pacific and the north Australian region associated with ENSO events may be smaller in a future climate.

This study has highlighted a link between tropical Pacific SSTs and those to the north of Australia, which could have important implications for the projections of Australian climate in a warming world. Understanding the physical mechanisms behind this link, and the processes that control it, will be an important next step in understanding the shortcomings of some of the current climate models, and how they may be improved. The ability of some climate models to reproduce the complex nature of the links between SSTs in the tropical Pacific and north of Australia suggests that data from these models may help us understand these physical mechanisms.

Acknowledgments. This study was supported by the Australian Research Council through the Linkage Project Grant LP0883961, the Discovery Project Grant DP0877417, and the ARC Centre of Excellence for Climate System Science (Grant CE110001028). NOAA ERSST V3 data were provided by the NOAA/OAR/ESRL PSD, Boulder, Colorado, from its website (at http://www.esrl.noaa.gov/psd/). HadISST data were provided by the Met Office Hadley Centre. Data were also provided by the British Atmospheric Data Centre (http://badc.nerc.ac.uk/view/badc.nerc.ac.uk__ATOM__dataent_hadisst). We acknowledge the modeling groups the Program for Climate Model Diagnosis and Intercomparison (PCMDI) and the WCRP's Working Group on Coupled Modelling (WGCM) for their roles in making available the WCRP CMIP3 multimodel dataset. Support of this dataset is provided by the Office of Science, U.S. Department of Energy. The authors wish to thank the three anonymous reviewers for their helpful comments.

REFERENCES

AchutaRao, K., and K. R. Sperber, 2002: Simulation of the El Niño Southern Oscillation: Results from the Coupled Model Intercomparison Project. *Climate Dyn.,* **19,** 191–209.

——, and ——, 2006: ENSO simulation in coupled ocean-atmosphere models: Are the current models better? *Climate Dyn.,* **27,** 1–15.

Alexander, L. V., and J. M. Arblaster, 2009: Assessing trends in observed and modelled climate extremes over Australia in relation to future projections. *Int. J. Climatol.,* **29,** 417–435.

Collins, M., and Coauthors, 2005: El Niño- or La Niña-like climate change? *Climate Dyn.,* **24,** 89–104.

DiNezio, P., A. Clement, and G. A. Vecchi, 2010: Reconciling differing views of tropical Pacific climate change. *Eos, Trans. Amer. Geophys. Union,* **91,** 141–142.

Guilyardi, E., 2006: El Niño-mean state-seasonal cycle interactions in a multi-model ensemble. *Climate Dyn.,* **26,** 329–348.

——, and Coauthors, 2004: Representing El Niño in coupled ocean–atmosphere GCMs: The dominant role of the atmospheric component. *J. Climate,* **17,** 4623–4629.

——, P. Braconnot, F.-F. Jin, S. Tae Kim, M. Kolasinski, T. Li, and I. Musat, 2009: Atmosphere feedbacks during ENSO in

a coupled GCM with a modified atmospheric convection scheme. *J. Climate,* **22,** 5698–5718.

Held, I. M., and B. J. Soden, 2006: Robust responses of the hydrological cycle to global warming. *J. Climate,* **19,** 5686–5699.

Joseph, R., and S. Nigam, 2006: ENSO evolution and teleconnections in IPCC's twentieth-century climate simulations: Realistic representation? *J. Climate,* **19,** 4360–4377.

Kug, J.-S., J. Choi, S.-I. An, F.-F. Jin, and A. T. Wittenberg, 2010: Warm pool and cold tongue El Niño events as simulated by the GFDL 2.1 coupled GCM. *J. Climate,* **23,** 1226–1239.

Leloup, J., M. Lengaigne, and J.-P. Boulanger, 2008: Twentieth century ENSO characteristics in the IPCC database. *Climate Dyn.,* **30,** 277–291.

Lloyd, J., E. Guilyardi, H. Weller, and J. Slingo, 2009: The role of atmosphere feedbacks during ENSO in the CMIP3 models. *Atmos. Sci. Lett.,* **10,** 170–176.

——, ——, and ——, 2010: The role of atmosphere feedbacks during ENSO in the CMIP3 models. Part II: Using AMIP runs to understand the heat flux feedback mechanisms. *Climate Dyn.,* **37,** 1271–1292.

Lu, J., G. A. Vecchi, and T. Reichler, 2007: Expansion of the Hadley cell under global warming. *Geophys. Res. Lett.,* **34,** L06805, doi:10.1029/2006GL028443.

——, G. Chen, and D. M. W. Frierson, 2008: Response of the zonal mean atmospheric circulation to El Niño versus global warming. *J. Climate,* **21,** 5835–5851.

Meehl, G. A., G. J. Boer, C. Covey, M. Latif, and R. J. Stouffer, 2000: The Coupled Model Intercomparison Project (CMIP). *Bull. Amer. Meteor. Soc.,* **81,** 313–318.

Min, S.-K., S. Legutke, A. Hense, and W.-T. Kwon, 2005: Internal variability in a 1000-yr control simulation with the coupled climate model ECHO-G – II. El Niño Southern Oscillation and North Atlantic Oscillation. *Tellus,* **57A,** 622–640.

Nakićenović, N., and R. Swart, Eds., 2000: *Special Report on Emissions Scenarios*. Cambridge University Press, 599 pp.

Neale, R. B., J. H. Richter, and M. Jochum, 2008: The impact of convection on ENSO: From a delayed oscillator to a series of events. *J. Climate,* **21,** 5904–5924.

Nicholls, N., 1984a: Seasonal relationships between Australian rainfall and north Australian sea surface temperature. *Extended Abstracts, Conf. on Australian Rainfall Variability,* Arkaroola, SA, Australia, Australian Academy of Science, 71–73.

——, 1984b: The Southern Oscillation and Indonesian sea surface-temperature. *Mon. Wea. Rev.,* **112,** 424–432.

——, 1984c: The Southern Oscillation, sea-surface-temperature, and interannual fluctuations in Australian tropical cyclone activity. *J. Climatol.,* **4,** 661–670.

——, 2010: Local and remote causes of the southern Australian autumn-winter rainfall decline, 1958–2007. *Climate Dyn.,* **34,** 835–845.

Ohba, M., and D. Nohara, 2010: Simulation of asymmetric ENSO transition in WCRP CMIP3 multimodel experiments. *J. Climate,* **23,** 6051–6067.

Power, S., M. Haylock, R. Colman, and X. Wang, 2006: The predictability of interdecadal changes in ENSO activity and ENSO teleconnections. *J. Climate,* **19,** 4755–4771.

Ramsay, H. A., L. M. Leslie, P. J. Lamb, M. B. Richman, and M. Leplastrier, 2008: Interannual variability of tropical cyclones in the Australian region: Role of large-scale environment. *J. Climate,* **21,** 1083–1103.

Randall, D. A., and Coauthors, 2007: Climate models and their evaluation. *Climate Change 2007: The Physical Science Basis,* S. Solomon et al., Eds., Cambridge University Press, 589–662.

Rasmusson, E. M., and T. H. Carpenter, 1982: Variations in tropical sea surface temperature and surface wind fields associated with the Southern Oscillation/El Niño. *Mon. Wea. Rev.,* **110,** 354–384.

Rayner, N. A., D. E. Parker, E. B. Horton, C. K. Folland, L. V. Alexander, D. P. Rowell, E. C. Kent, and A. Kaplan, 2003: Global analyses of sea surface temperature, sea ice, and night marine air temperature since the late nineteenth century. *J. Geophys. Res.,* **108,** 4407, doi:10.1029/2002JD002670.

Roberts, M. J., and Coauthors, 2009: Impact of resolution on the tropical Pacific circulation in a matrix of coupled models. *J. Climate,* **22,** 2541–2556.

Smith, T. M., R. W. Reynolds, T. C. Peterson, and J. Lawrimore, 2008: Improvements to NOAA's historical merged land–ocean surface temperature analysis (1880–2006). *J. Climate,* **21,** 2283–2296.

Taylor, K. E., 2001: Summarizing multiple aspects of model performance in a single diagram. *J. Geophys. Res.,* **106** (D7), 7183–7192.

Torrence, C., and P. J. Webster, 1998: The annual cycle of persistence in the El Niño/Southern Oscillation. *Quart. J. Roy. Meteor. Soc.,* **124,** 1985–2004.

Ummenhofer, C. C., A. Sen Gupta, M. J. Pook, and M. H. England, 2008: Anomalous rainfall over southwest Western Australia forced by Indian Ocean sea surface temperatures. *J. Climate,* **21,** 5113–5134.

van Oldenborgh, G. J., S. Y. Philip, and M. Collins, 2005: El Niño in a changing climate: A multi-model study. *Ocean Sci.,* **1,** 81–95.

Wang, X., D. Wang, and W. Zhou, 2009: Decadal variability of twentieth-century El Niño and La Niña occurrence from observations and IPCC AR4 coupled models. *Geophys. Res. Lett.,* **36,** L11701, doi:10.1029/2009GL037929.

Wittenberg, A. T., A. Rosati, N.-C. Lau, and J. J. Ploshay, 2006: GFDL's CM2 global coupled climate models. Part III: Tropical Pacific climate and ENSO. *J. Climate,* **19,** 698–722.

Xue, Y., T. M. Smith, and R. W. Reynolds, 2003: Interdecadal changes of 30-yr SST normals during 1871–2000. *J. Climate,* **16,** 1601–1612.

Zhang, Y., H. Wang, J. Sun, and H. Drange, 2010: Changes in the tropical cyclone genesis potential index over the western North Pacific in the SRES A2 scenario. *Adv. Atmos. Sci.,* **27,** 1246–1258.